Design of Robust AMB Controllers for Rotors Subjected to Varying and Uncertain Seal Forces

Lauridsen, Jonas Skjødt; Santos, Ilmar

Published in:
Mechanical Engineering Journal

Link to article, DOI:
10.1299/mej.16-00618

Publication date:
2017

Document Version
Publisher's PDF, also known as Version of record

Bulletin of the JSME Vol.4, No.5, 2017
Mechanical Engineering Journal

Design of robust AMB controllers for rotors subjected to varying and uncertain seal forces

Jonas LAURIDSEN* and Ilmar SANTOS*
* Dept. of Mechanical Eng., Technical University of Denmark
Copenhagen, Denmark
E-mail: ifs@mek.dtu.dk

Received: 16 November 2016; Revised: 19 April 2017; Accepted: 8 May 2017

Abstract
This paper demonstrates the design and simulation results of model based controllers for AMB systems, subjected to uncertain and changing dynamic seal forces. Specifically, a turbocharger with a hole-pattern seal mounted across the balance piston is considered. The dynamic forces of the seal, which are dependent on the operational conditions, have a significant effect on the overall system dynamics. Furthermore, these forces are considered uncertain. The nominal and the uncertainty representation of the seal model are established using results from conventional modelling approaches, i.e. Computational Fluid Dynamics (CFD) and Bulkflow, and experimental results. Three controllers are synthesized: I) An $\mathcal{H}_\infty$ controller based on nominal plant representation, II) A μ controller, designed to be robust against uncertainties in the dynamic seal model and III) a Linear Parameter Varying (LPV) controller, designed to provide a unified performance over a large operational speed range using the operational speed as the scheduling parameter. Significant performance improvement is shown for robust control, incorporating model uncertainty, compared to nominal model based control.

Keywords : Uncertain dynamic seal forces, Robust control, LPV control, AMB, Turboexpander, Hole-pattern seal, Fluid interaction

1. Introduction

Annular seals in rotordynamic systems can generate significant dynamic forces, and under certain conditions, destabilize the system leading a to machine failure. In rotordynamic systems supported by Active Magnetic Bearings (AMBs) these forces can, to a certain degree, be compensated for by employing appropriate feedback controllers. However, incorporating seal dynamics into the control design can be challenging due to, among other things, the frequency dependence of seal forces, varying operating conditions, process fluid characteristics and model uncertainties.

A number of publications have been presented focusing on the mathematical description of seal dynamics using either CFD or empirically-based Bulkflow models, and it has been shown that for seals under well defined single phase conditions a reasonable match between theoretical and experimental results can be achieved (Nielsen et al., 2012). However, seal dynamics under multiphase conditions, i.e. where the fluid is a mixture of gas and liquid, are still challenging. Larger model uncertainties should be expected for seals under multiphase conditions due to a limited knowledge of the dynamic behaviour of such fluids, especially when combined with complex seal geometries such as hole-pattern and labyrinth. Model uncertainties are thus inevitable due to these limitations of the mathematical models. Furthermore, seal model parameters change depending on operational conditions such as rotational speed and pressure difference across the seal.

A large quantity of research has focused on designing robust control for AMB systems. A popular choice for designing robust Linear Time Invariant (LTI) controllers for AMB systems is by using the $\mathcal{H}_\infty$ framework and an Linear Fractional Transformation (LFT) formulation to represent the nominal system and uncertainty.

Paper No.16-00618
J-STAGE Advance Publication date: 17 May, 2017
[DOI: 10.1299/mej.16-00618]

Using $\mathcal{H}_\infty$ with an uncertainty representation of the plant, the controller is directly synthesized to ensure a satisfactory worst case performance. The conservativeness of the synthesised $\mathcal{H}_\infty$ controller can in many cases be reduced using DK-iteration, as done using the μ-synthesis framework (Zhou et al., 1996).

A side benefit of using the $\mathcal{H}_\infty$ framework for synthesising controllers for AMB based systems is the ability to optimize the response due to worst case mass unbalance distribution. Singular Value Decomposition (SVD) can be used as a worst case measure, since the actual distribution of mass unbalance is unknown in terms of magnitude and phase. This can be applied for control synthesis shown in (Schweitzer et al., 2009) as well as for analysis shown in (Cloud et al., 2005) and with application to a subsea compressor with a flexible rotor (Maslen et al., 2012).

The robustness criteria for AMB systems are specified as the sensitivity (ISO 14839-3, 2006), stating that the closed loop sensitivity should be less than 3 for the system to be classified as Class A. Also this requirement can explicitly be dealt with using $\mathcal{H}_\infty$, by weighting the sensitivity function.

Balas & Young (1995) show that robust controllers for uncertain rotational speed can be addressed using a LFT consisting of the nominal system, a representation of how the system changes due to gyroscopic effects and a repeated uncertainty. In (Schonhoff et al., 2000) uncertainties of the natural frequencies of the flexible shaft's bending modes are considered and a robust controller is designed using μ synthesis. Robust stability to additive and multiplicative uncertainties can directly be ensured by applying complex weighting functions to the transfer functions KS (controller sensitivity) and T (complementary sensitivity). The conservativeness of the robust controller design can be reduced in the case of Linear Parameter Varying (LPV) controller design, where one or more parameters are measured in real time, and can represent changing dynamics, which otherwise would be considered uncertain. A measured parameter could be the rotation speed, which can be utilized to reduce synchronous vibrations as shown in (Balini et al., 2012).

In (Mushi et al., 2008) a system consisting of a flexible rotor subjected to cross coupled stiffness (CCS) is considered theoretically and experimentally. The CCS is generated using an extra set of AMBs. It is found that it is very hard to design robust controllers using μ-synthesis that can compensate for uncertain cross coupled stiffness specifically for the flexible rotor system considered in the work.

In (Pesch & Sawicki, 2015) a μ controller is designed to control the oil whip and oil whirl occurring from a journal bearing using AMBs. The idea is to use the journal bearing to provide high load capacity and the AMB to increase stability margin. The controller is based on the Bently-Muszynska fluid film bearing model to predict the unstable bearing behaviour and is designed to be robust due to angular velocity changes. Experimental results shows that the controller increases the stability margin significantly. It is, however, challenging in the case of such a hybrid bearing system to balance the load sharing between the journal and magnetic bearings such that they do not counteract each other. This can be explained by considering the equilibrium positions of each of the journal and magnetic bearings. In the case of the journal bearing, the equilibrium position changes with rotor angular velocity due to the interactions between the rotor and the fluid film, and may not be precisely known in advance. On the other hand, an AMB equilibrium position is traditionally controlled to a fixed reference point. However, it is desirable that the AMB equilibrium position is constantly adjusted to align with the (varying) equilibrium position of the journal bearing, such that the journal bearing is always supporting the static load, while the AMB acts purely as an active control actuator, providing zero static force. This issue is recently addressed in (Caple et al., 2016) in which a method is presented to enable the AMB to adapt its bias distribution to produce a zero static force, using a low frequency periodic bias carrier signal. The idea is conceptually sound, although simulation results show that several issues regarding this approach still needs to be addressed. One issue is that a residual coupling between the carrier signal and the control signal can result to unintended excitation of lightly damped flexible modes. Another example of hybrid bearing can be found in (Jeong et al., 2016). Here the AMB and controllers is designed to operate along with air foil bearings.

Adaptive controllers to detect and compensate for CCS forces have been reported. Wurmsdobler & Springer (1996) presents simulation results of a rotordynamic system supported by AMBs and subjected to a time invariant CCS magnitude. An observer is constructed and shows the ability to track the changing CSS magnitude over time. A controller designed using pole placement technique was designed to work along with the observer. Similar work is shown in (Lang et al., 1996) but here the unknown CSS parameter of a rotor are estimated on-line by a standard least-square estimator along with a time-varying forgetting factor. Simulation results of adaptive control in parallel with a baseline PID controller is considered in (Hirschmanner & Springer 2002) of

[DOI: 10.1299/mej.16-00618]

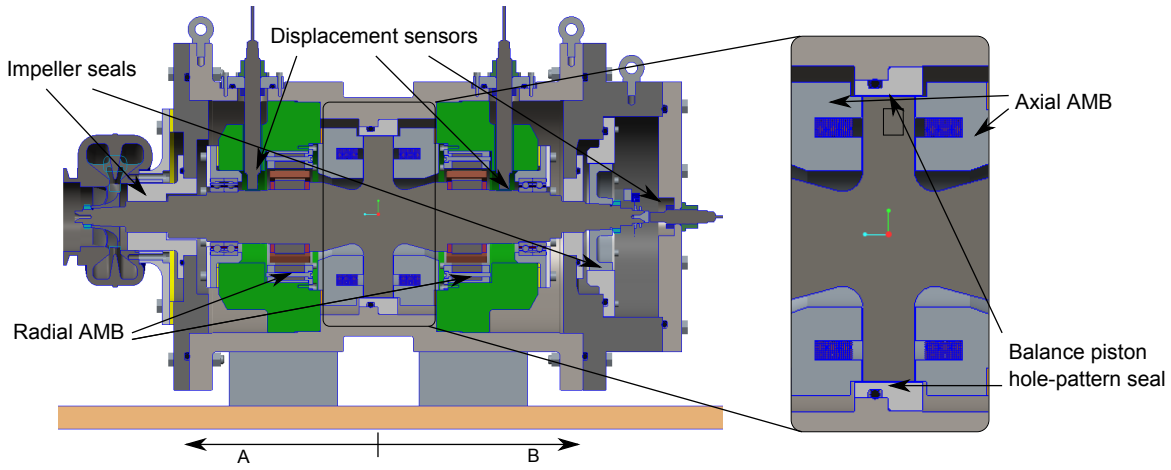

Fig. 1 Cross section of the turboexpander testrig. An enlargement of the center section section shows the balance piston on which the axial bearings acts and where the hole-pattern seal are placed

a non-linear simulation model. Here the controller is designed to compensate changing CCS magnitude over time as well as to compensate for periodic disturbance forces. The work shows that the adaptive controller can handle much larger amplitudes of CCS forces than a LTI LQR compensator. However, only numerical studies have been carried out so far on the adaptive controllers. Stability and robustness is in general hard to guarantee in adaptive control systems, which of course is crucial for implementation in industrial applications.

This paper presents a mathematical model of a high speed turboexpander unit used for cryogenic air separation and the design of model-based feedback controllers for the pair of radial AMBs responsible for magnetic levitation and stabilization. One hole-pattern seal is placed across a balance piston in the center of the turboexpander generating a thrust force to oppose the sum of the impeller thrust forces. The seal dynamics are considered uncertain and further changes due to operating conditions. A robust LTI controller is designed using μ synthesis to compensate for uncertain seal forces and is compared to an $\mathcal{H}_\infty$ controller based on the nominal model. For improved performance, an LPV controller is designed, which schedules controllers depending on the rotational speed. A performance comparison between the controllers based on the nominal model, the uncertain system representation and parameter varying model is presented.

2. Modelling of the Turboexpander

A cross-section schematic of the turboexpander investigated is shown in Fig. 1. The turboexpander essentially consists of a shaft levitated using axial and radial AMBs, and three annular seals. It is assumed that the only significant forces acting on the rigid rotor are the left and right side radial AMB and the seal in the center. The displacement sensors are placed close to the AMBs. The axial placement of the sensors and actuators are denoted by A and B, indicated in Fig. 1, with subscript x, y indicating the radial movement in the global horizontal and vertical coordinate system. The analysis will be focused on rotor lateral movements; for simplicity the rotor axial movements will not be investigated. The term AMB will therefore refer to the radial AMBs in the rest of this work.

2.1. AMB Model

The model of the magnetic bearing is simplified to describe the forces acting on the rotor as function of the rotor lateral displacements to AMB s_x and the control current i_x. The linearised expression of the forces are given as

$$f_b(i_x, s_x) = K_i i_x + K_s s_x \tag{1}$$

where K_i are K_s are constants. The dynamics of the electromechanical system, including the inductance of the coil and the amplifiers, is approximated as a first order system with a 3 dB cut-off frequency ω_c at 1.5 kHz, denoted G_{act}.

[DOI: 10.1299/mej.16-00618]

$$G_{act} = \frac{K_i}{1 + \frac{s}{\omega_c}} \tag{2}$$

2.2. Model of Shaft

The rotating shaft is modelled using the Finite Element (FE) method and Bernoulli-Euler beam theory taking into account the gyroscopic effects of the shaft and discs (Nelson, 1980). The shaft model is discretized into 40 node points with 4 degrees of freedom each, i.e. x and y direction, and the rotation around the x and y axes, which yields 320 states in total. The full order rotordynamic system G_f consisting of the finite element model of the shaft and negative stiffness forces from the AMB can be written in state space form

$$\dot{x}_f = A_f x_f + B_f u, \quad y = C_f x_f \tag{3}$$

Using modal truncation techniques, real left and right modal transformation matrices are obtained which transform the full order FE system to a reduced form, shown in Eq. (4). The first bending mode of the shaft lies at approx. 1 kHz. Since this is substantially above the frequency range of interest in this work, the shafts is assumed rigid and all bending modes have thus been removed in the reduced order model. The FE model is selected though for generality and for possibility of to extend the model to included some of the bending modes if needed.

$$x = {T_L}^T x_f, \quad A = {T_L}^T A_f T_R, \quad B = {T_L}^T B_f, \quad C = C_f T_R \tag{4}$$

2.3. Seal Model - CFD vs Bulkflow

CFD and Bulkflow methods are typically used to obtain the static and dynamic properties of seals. CFD has been shown to be able to find seal forces even with complex geometries but can be extremely time demanding and computational heavy, since full 3D flow and pressure fields have to be calculated. On the other hand Bulkflow models are much simpler since these are based on simplified 1D models heavily linked to empirical parameters. The results of both CFD and Bulkflow modelling are usually validated against experimental data. Industrial software like ISOTSEAL is based on Bulkflow models and is widely used in the industry. Independent of the modelling approach, the dynamic seal forces are usually represented by their linearised force coefficients: stiffness, damping and sometimes mass matrices:

$$\begin{bmatrix} f_x \\ f_y \end{bmatrix} = \begin{bmatrix} K & k \\ -k & K \end{bmatrix} \begin{bmatrix} x \\ y \end{bmatrix} + \begin{bmatrix} C & c \\ -c & C \end{bmatrix} \begin{bmatrix} \dot{x} \\ \dot{y} \end{bmatrix} + \begin{bmatrix} M & 0 \\ 0 & M \end{bmatrix} \begin{bmatrix} \ddot{x} \\ \ddot{y} \end{bmatrix} \tag{5}$$

This model has a symmetric structure since the shaft is assumed to be approximately in the center. The sign difference of the cross coupled stiffness and damping coefficients is commonly known to cause instability. The coefficients are a function of the rotational speed and the excitation frequency. The seal used in the turboexpander application is a hole-pattern seal with coefficients taken from (Nielsen et al., 2012). The coefficients are given for a constant rotational speed of 20,200 RPM and with excitation frequencies varying from 20-300 Hz, and the specifications are stated in Fig. 2. The stiffness and damping coefficients are shown in Fig. 3 & 4 and are found using CFD, ISOTSEAL and experimental work originating from Turbolab (Nielsen et al., 2012; Dawson et al., 2002). The estimated model uncertainty between the CFD and experimental results is marked as the grey area in the figures, and this information is utilized when synthesizing robust controllers. In the case of using ISOTSEAL as a nominal seal model, larger uncertainties must be expected and hence included in the uncertainty model.

3. Robust Control Design

In this section a robust controller is designed using μ synthesis to handle realistic uncertainties and changes in the seal dynamics. This controller is compared to a $\mathcal{H}_\infty$ controller based on a nominal system model.

3.1. Control Design Objectives and Challenges

- Due to model uncertainties and changes in operational conditions, the controller should deliver robust performance to plants with seal stiffness and damping coefficients within ±40 % of the nominal values. All

[DOI: 10.1299/mej.16-00618]

Parameter	Value
Seal Length [mm]	85.70
Rotor Diameter [mm]	114.74
Inlet Clearance [mm]	0.2115
Exit Clearance [mm]	0.2102
Hole Depth [mm]	3.30
Hole Diameter [mm]	3.18
Hole Area Ratio	0.684
Rotor Speed [rpm]	20200
Inlet Pressure [bar]	70.0
Outlet Pressure [bar]	31.5
Res. Temperature [C]	17.4
Preswirl	0

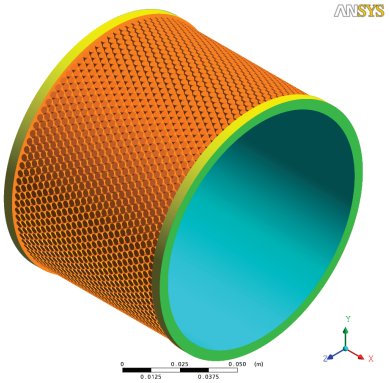

Fig. 2 Hole-pattern seal specification and parameters (left) & fluid structure (right). From (Nielsen et al., 2012)

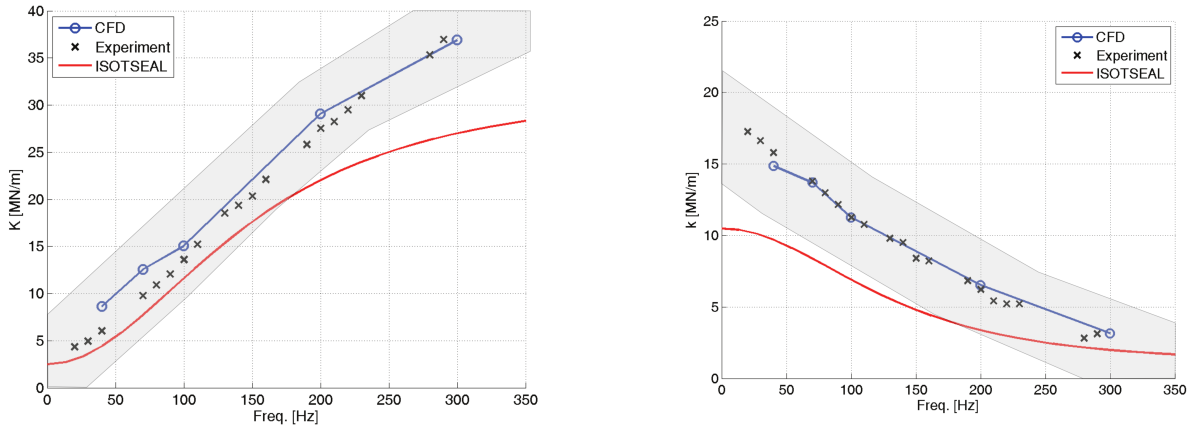

Fig. 3 Hole-pattern seal direct and cross coupled stiffness coefficients obtained using CFD, Experiment and ISOTSEAL. Figures adapted from (Nielsen et al., 2012)

8 coefficients are considered uncertain independent to each other, i.e. although, for example, the direct coupled stiffness K has the same nominal value in both vertical and horizontal directions they have independent uncertainties. Mass coefficients are neglected since the fluid is air (Nielsen et al., 2012).

- The system should be robust against other unmodelled dynamics and against system changes over time due to wear and ageing. These robustness criteria are specified in ISO 14839-3, which states that the closed loop sensitivity (disturbance to error) should be less than 3 for all frequencies in order to be classified as Zone A (ISO 14839-3, 2006).
- Unbalance response should be less than $10\,\mu$m for the complete operating range, assuming the shaft is balanced according to the G2.5 standard.
- The control currents should stay well within the actuation limits of ± 5 A.
- Settling time should be less than 20 ms for step disturbances on input (force) for good force disturbance rejection.

3.2. Uncertainty Representation

The nominal rotordynamic model consists of the reduced order shaft model, the negative stiffness from the AMBs and the nominal stiffness and damping from the seals. The perturbation model G_{fi} is constructed using the nominal model and the uncertainty representation, which are combined and written in LFT form, illustrated in Fig. 5. Here Δ is a 8×8 diagonal matrix representing the normalized uncertainties and satisfy $\|\Delta\|_\infty \leq 1$. G_{fi} can be written in state space form, as shown in Eq. (6), where A, B and C are the nominal system matrices. Here the input and output matrices are extended from the nominal model to include the input and output mapping B_Δ and C_Δ. Note that no extra system dynamics is added since the LFT only changes the

[DOI: 10.1299/mej.16-00618]

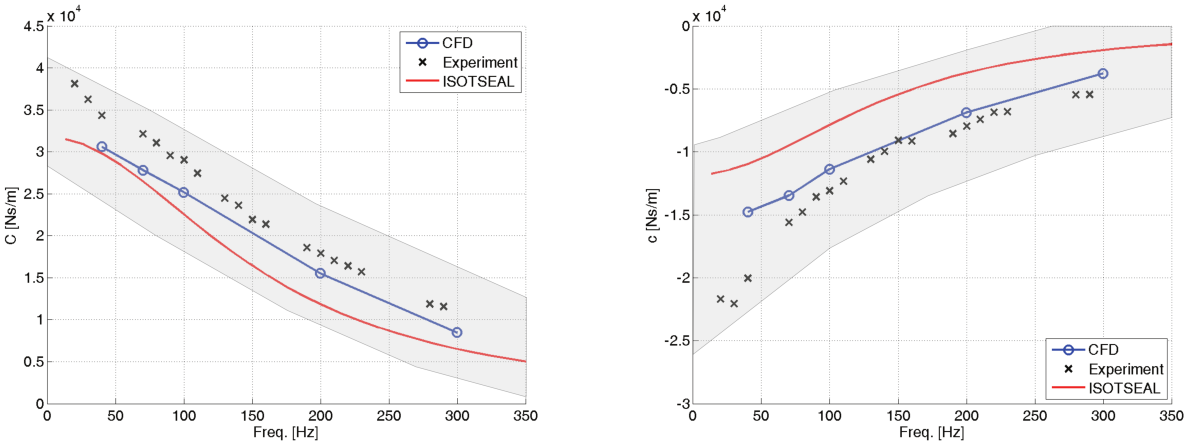

Fig. 4 Hole-pattern seal direct and cross coupled damping coefficients obtained using CFD, Experiment and ISOTSEAL. Figure adapted from (Nielsen et al., 2012)

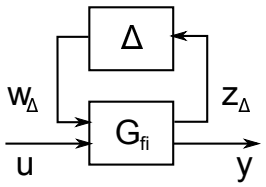

Fig. 5 Uncertain plant representation using upper LFT, $G_{unc} = \mathcal{F}_u\left(G_{fi}, \Delta\right)$

nominal system matrix A.

$$G_{fi} = \left[\begin{array}{c|cc} A & B_\Delta & B \\ \hline C_\Delta & 0 & 0 \\ C & 0 & 0 \end{array}\right] \tag{6}$$

B_Δ and C_Δ are constructed as follows and a thorough description of this process can be seen in (Lauridsen et al., 2015). It can be shown that changes in stiffness (or damping) in a single direction at e.g. A_x corresponds to a change in a single column of system matrix A, which corresponds to the node j where the stiffness (or damping) is altered.

$$A_{\Delta_f} = \begin{bmatrix} 0 & \dots & 0 & a_{1,j} & 0 & \dots & 0 \\ 0 & \dots & 0 & a_{2,j} & 0 & \dots & 0 \\ \vdots & \ddots & \vdots & \vdots & \vdots & \ddots & \vdots \\ 0 & \dots & 0 & a_{i,j} & 0 & \dots & 0 \end{bmatrix} \tag{7}$$

The change of the system matrix in reduced form A_Δ is found using the same modal truncation matrices as used to reduce the nominal system, as shown in Eq. (8). It is noted that the applicability of using the same modal truncation matrices to reduce the matrix representing the change in system dynamics – as were used for reducing the nominal system matrix – is based on assumption rather than proof, however, this assumption has been shown to hold well in practice. A_{Δ_f} in Eq. (7) can also be written as a column vector B_{Δ_f} and a row vector C_{Δ_f} and the change/uncertainty Δ. The input mapping B_Δ and output mapping C_Δ of the uncertainties are thus given as shown in Eq. (10). Repeating this process 8 times (one for each stiffness and damping parameter) and assembling the coloums of B_Δ and rows of C_Δ and making Δ an 8×8 diagonal matrix, yields the complete uncertainty representation.

$$A_\Delta = T_L\, A_{\Delta_f}\, T_R \tag{8}$$

$$= T_L B_{\Delta_f}\, \Delta\, C_{\Delta_f} T_R \tag{9}$$

$$= B_\Delta\, \Delta\, C_\Delta \tag{10}$$

[DOI: 10.1299/mej.16-00618]

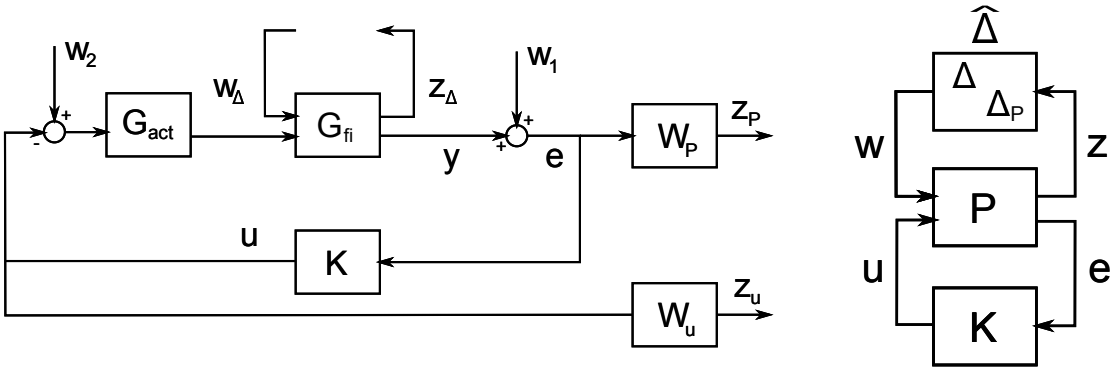

Fig. 6 Left figure: Interconnection of actuator model G_{act}, rotordynamic model with uncertainty representation G_{fi}, performance weight functions W_P and W_u, and controller K. Right figure: interconnection rearranged to the augmented system P, externally connected to the controller and $\hat{\Delta}$ containing Δ for uncertain plant representation and Δ_P as full complex perturbation for performance specification.

3.3. Robust Control Design Interconnection and Weight Functions

The interconnection in Fig. 6 is used for robust controller synthesis, This is similar to the structure suggested in (Balini et al., 2012). W_p shapes the sensitivity functions i.e. the relationship from input and output disturbances W_1 and W_2 to the displacement error e. W_p is formulated with the structure suggested in (Skogestad & Postlethwaite, 2007)

$$W_p = \frac{\frac{s}{M} + w_B}{s + w_B A} \tag{11}$$

The inverse of W_p is shown in Fig. 7 and the weighting function has multiple purposes: I) Set a low sensitivity at low frequencies to obtain an integral effect, which eliminates steady state error in position reference. A indicates the steady state error and is set to $\frac{1}{1000}$. II) M indicates the maximum peak of the sensitivity functions and is tuned to obtain an peak less than 3 (or 9.5 dB) for robustness. III) The crossover frequency w_B indicates the desired bandwidth of the closed loop system (Skogestad & Postlethwaite, 2007). This parameter is tuned to achieve a disturbance settling time of less than 20 ms. The weight W_u is a high-pass filter with a crossover frequency at 1.4 kHz which limits the bandwidth of the control action. The inverse of W_u is shown in Fig. 8.

3.4. Robust Control Synthesis

Fig. 6 (right) shows the interconnection rearranged for controller synthesis such that P is the fixed augmented plant. Note that Δ for uncertain plant representation and Δ_P (full perturbation matrix representing the $\mathcal{H}_\infty$ performance specification) are collected into the diagonal elements of $\hat{\Delta}$. Hence synthesising a controller can be done by finding a controller that minimises the ∞ norm of the transfer function from w to z, formulated as a lower LFT

$$\gamma = \|F_l(P, K)\|_\infty \tag{12}$$

The uncertainty is scaled to 1, meaning that robust performance is met when γ is below 1. γ larger than 1 means that either the uncertainty, the performance weights or both should be scaled by $\frac{1}{\gamma}$ for the solution to hold. Solving Eq. (12) using $\mathcal{H}_\infty$ synthesis resulted in a $\mathcal{H}_\infty$ controller with γ of 618. Since this is far above 1, this controller does not guarantee robust performance.

Reduce Conservatism by D-scaling Using $\mathcal{H}_\infty$ directly on the problem in Fig. 6 (right) is known to suffer from conservatism since the $\hat{\Delta}$ would be considered to be a full order complex perturbation. This is commonly solved using DK-iteration, where a scaling matrix D is found, scaling w and z by D and D^{-1} to reduce the conservatism. The D matrix is found using μ synthesis in Matlab which results in a performance index of 1.1, meaning that the system nearly guarantees robust performance.

3.5. Results

The input and output closed loop sensitivity functions, S_i and S_o, with parameter variations of ±40 % relative to the nominal plant are shown in Fig. 7 (left) using an $\mathcal{H}_\infty$ controller based on a nominal plant and

[DOI: 10.1299/mej.16-00618]

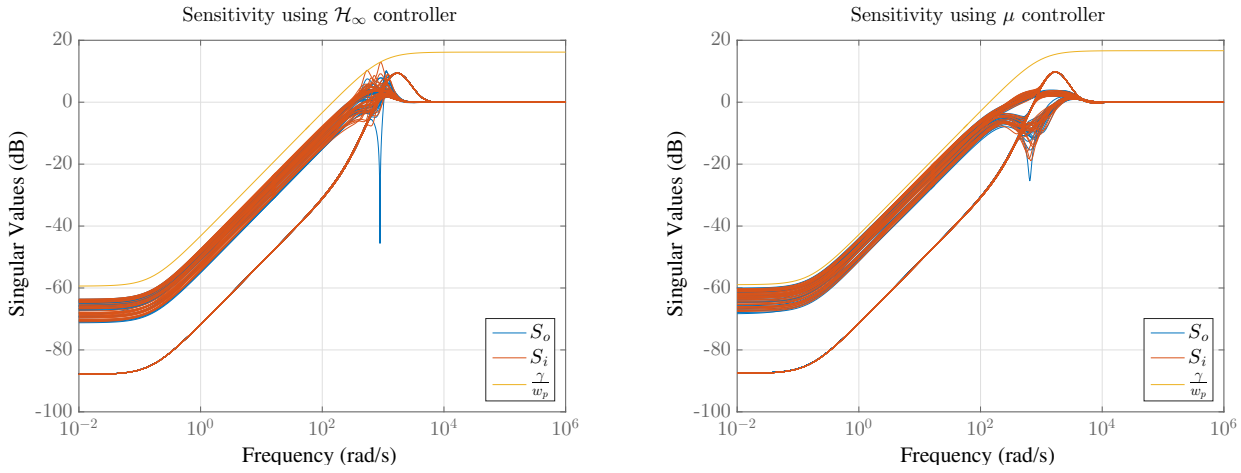

Fig. 7 Closed-loop sensitivity using $\mathcal{H}_\infty$ synthesized controller based on nominal plant (left) and using μ synthesized controller based on perturbation plant (right)

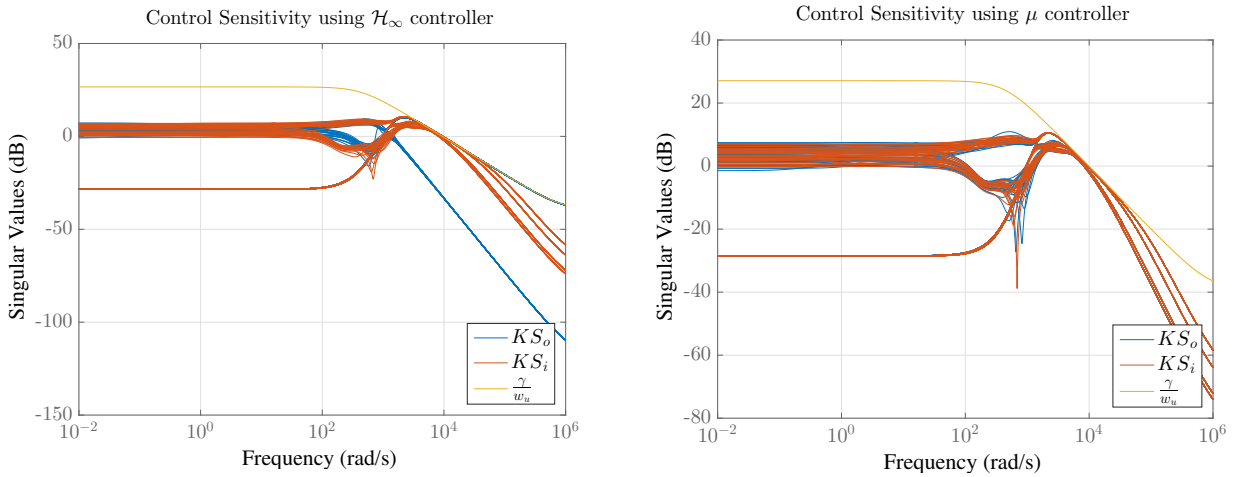

Fig. 8 Closed-loop control sensitivity using $\mathcal{H}_\infty$ synthesized controller based on nominal plant (left) and using μ synthesized controller based on perturbation plant (right)

is shown in Fig. 7 (right) using μ synthesized controller based on the uncertain plant representation. The sensitivity peak is above 10 dB using the $\mathcal{H}_\infty$ controller based on nominal plant, and thus does not meet the requirements. The closed loop control sensitivity functions, KS_i and KS_o, with parameter variations of ±40 % relative to nominal plant are shown in Fig. 8 (left) using an $\mathcal{H}_\infty$ controller based on a nominal plant and is shown in Fig. 8 (right) using μ synthesized controller based on the uncertain plant representation. Both controllers stays within the weight function limits and stays within the bandwidth requirements.

Fig. 9 and Fig. 10 shows the displacement and control currents of an impulse response of the closed loop system. Nodes A_x, A_y, B_x and B_y are the locations of AMB A and B. The impulse disturbance has an amplitude of 100 N and length of 2 ms and enters through node A_x. Multiple simulations are shown for different parameter variations within ±40 %. It is clearly seen that the μ controller delivers consistent robust performance, whereas the $\mathcal{H}_\infty$ controller does not, even turning unstable for some parameter variations. It is observed that although the system is disturbed in x-direction, there is also movement in y-direction due to cross-coupling from the seal and gyroscopic forces.

Worst Case Unbalance Response The compliance function, denoted $G_f(\Delta)$, maps the external force disturbance input to the rotor displacement

$$G_f(\Delta) = \mathcal{F}_u\left(G_{fi}, \Delta\right) S_i \tag{13}$$

A low compliance function indicates good force disturbance rejection. Finding the maximum singular values of the compliance function multiplied by the unbalance force $F_u(\Omega)$ yields a conservative indication of the worst

[DOI: 10.1299/mej.16-00618]

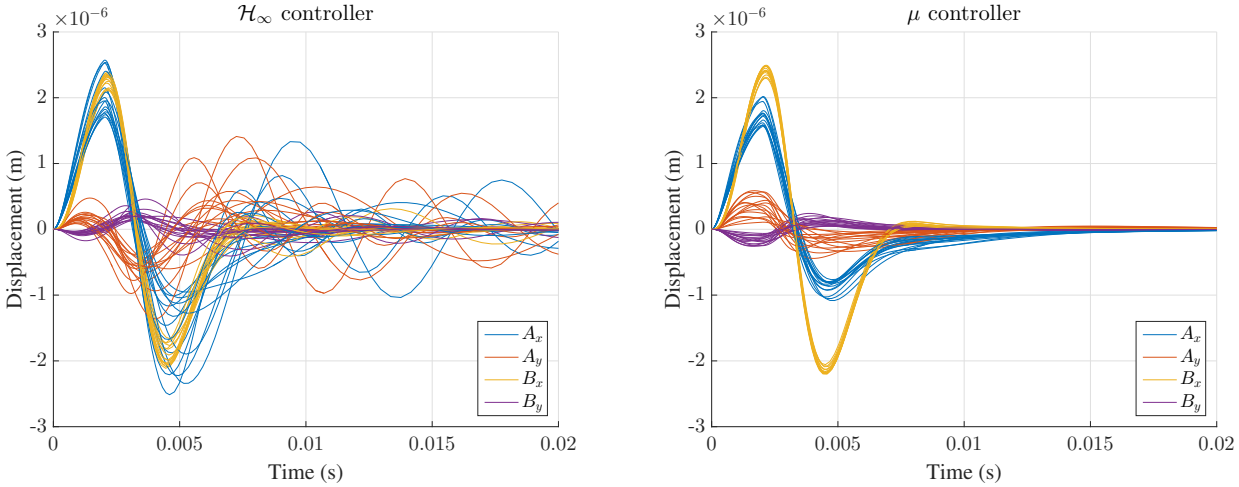

Fig. 9 Impulse response using $\mathcal{H}_\infty$ synthesized controller based on nominal plant (left) and using μ synthesized controller based on perturbation plant (right)

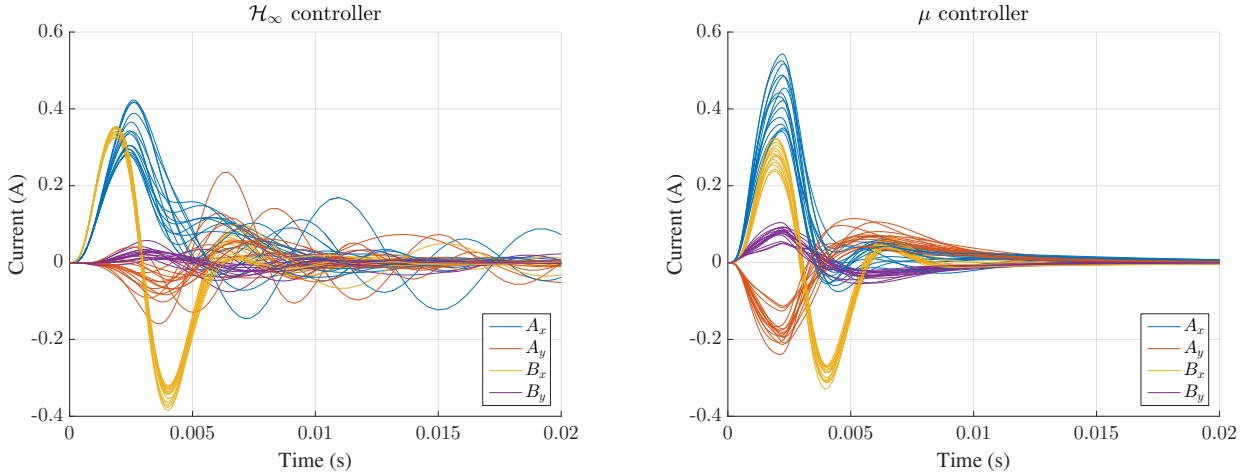

Fig. 10 Control action in response to an impulse disturbance using $\mathcal{H}_\infty$ synthesized controller based on nominal plant (left) and using μ synthesized controller based on perturbation plant (right)

case unbalance response y_{max} due to uncertain seal forces

$$y_{max} = \bar{\sigma}(G_f(\Delta))F_u(\Omega) \quad \forall\Omega \tag{14}$$

Where Ω is the rotational speed and $F_u(\Omega)$ is given by the $G2.5$ unbalance specification. Solving (14) numerically for Ω within the range 20-300 Hz, using the μ controller, shows that displacement stays within 4 μm for ±40 % parameter variations and thus meets the requirements.

4. LPV Control Design

A Linear Parameter Varying (LPV) controller is synthesized using the Linear Matrix Inequality (LMI) formulation from (Apkarian & Adams, 1998) and using the control interconnection and weighting functions shown in Fig. 6. However, instead of using the perturbed plant representation G_{fi}, a LPV plant is used for control synthesis and simulation. For this case study it is assumed that the coefficients for the hole pattern seal over the excitation frequency range of 20-300 Hz represents the synchronous coefficients for the rotational speed range of 20-300 Hz.

Results of Spin-up Test - LPV vs μ Controller A spin-up simulation response, demonstrating the performance of the LPV and μ controller over the operating range of 20-300 Hz with a duration of 1 s, is carried out. The μ controller is designed for an operational speed of 140 Hz and to deliver robust performance to plants with seal stiffness and damping coefficients within ±40 % of the nominal values. Step disturbances are applied every 50 ms,

[DOI: 10.1299/mej.16-00618]

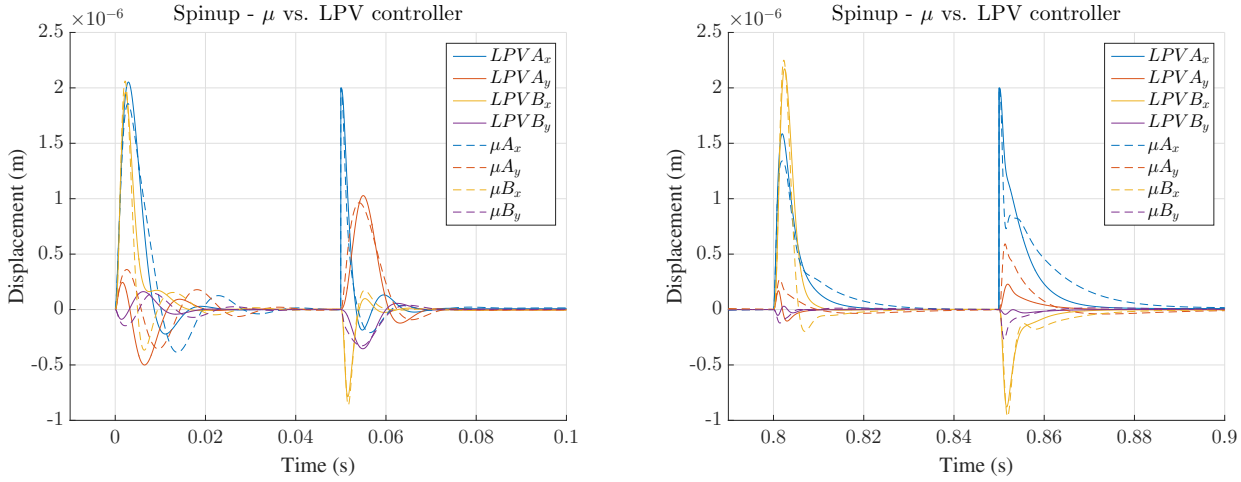

Fig. 11 Spin-up test time response comparison, using LPV and μ controllers. A force input disturbance of 100 N enters after 0 s and 0.8 s and a displacement output disturbance of 2 μm enters after 0.05 s and 0.85 s, both at A_x. The μ controller is designed for operation at 140 Hz rotational speed.

alternating between acting on the input and output signals. A force input disturbance of 100 N enters after 0 s and a displacement output disturbance of 2 μm enters after 50 ms, both at A_x. The μ controller performs, not surprisingly, best near its design operational point at 140 Hz and worse when operating away from it. Worst case performance of the μ controller is illustrated in Fig. 11 (left) for low operational speeds in the beginning of the spinup and in Fig. 11 (right) for high operational speeds. It is observed, that for these operational ranges, the LPV controller has a faster settling time, below 20 ms as required, where the μ controller takes longer time. Also, the response is more oscillatory in the case of the μ synthesized controller compared to the LPV controller.

Fig. 12 shows S_o using LPV and μ controllers for plant variations due to plant changes in the operational speed range of 20-300 Hz. The plot confirms worse performance of the μ synthesized controller, i.e: I) Oscillatory behaviour due to higher peak of S_o. II) Slower disturbance rejection due to lower crossover frequency.

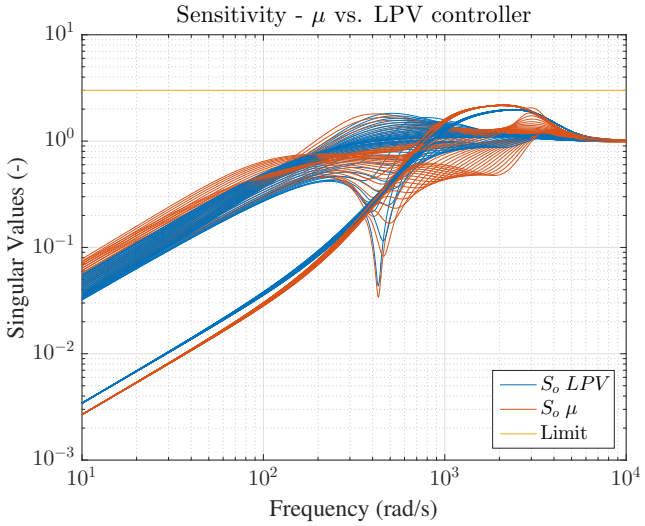

Fig. 12 Closed loop output sensitivity using LPV and μ controllers for plant variations due to change in operational speed in the range 20-300 Hz. The yellow line indicates the ISO14839-3 upper limit.

5. Conclusion

Robust control design is suggested for handling uncertain seal forces in AMB systems. Significant performance improvement is shown for robust control, incorporating model uncertainty, compared to nominal model based control. This clearly demonstrates the need for incorporating uncertainties into the model based con-

[DOI: 10.1299/mej.16-00618]

troller design process to obtain robust performance. The μ controller is minimally conservative to the known uncertainty structure.

In the case of significant frequency dependence of the dynamic seal characteristics, as for the hole pattern seal, combined with large variations in operational speed, it is more challenging to design a single robust LTI controller that provides satisfactory performance over the complete operational range. This paper demonstrates the performance improvement an LPV controller can deliver, compared to a single robust LTI controller, using the nominal plant model. The best robust controller that was designed for the whole rotational speed range used a nominal plant representation for the seal dynamics using the average speed of 140 Hz. While this controller actually meets the ISO requirements for the complete operating range, this controller shows a decreased performance, especially away from its operating point. For simplicity, robustness due to uncertainties is not considered when comparing the μ and LPV controller over the complete operational range. It would, however, be more challenging to design controllers which deliver satisfactory performance for plants that can change both due to the operational speed and uncertainties. The uncertainty representation can be integrated into the LPV synthesization, although this would make the synthesization computationally heavier and possibly more sensitive to numerical instabilities.

One of the advances by using the LPV framework for synthesizesing controllers is the possibility to guarantee stability due to fast changes in plant dynamics simultaneously with fast switching between controllers. The LPV controller in this paper is designed to guarantee stability due changes that can be infinitely fast. This typically introduces some conservativeness since the rotational speed changes in the physical plant are in reality limited due to the inertia of the shaft. Thus, the performance of the LPV controller can possibly be improved by imposing boundaries on the velocity. This can be done by making the Lyapunov function variables depended on the scheduling parameter. This would, however, increase the complexity of the synthesization.

References

Apkarian, P. and Adams, R. J., Advanced gain-scheduling techniques for uncertain systems, Control Systems Technology, IEEE Transactions on Vol.6, No.1 (1998), pp.21-32.

Balas, G. J. and Young, P. M., Control design for variations in structural natural frequencies, Journal of Guidance, Control and Dynamics Vol.18, No.2 (1995), pp.325-332.

Balini, H. M. N. K., Witte, J. and Scherer, C. W., Synthesis and implementation of gain-scheduling and LPV controllers for an AMB system, Automatica Vol.48, No.3 (2012), pp.521-527.

Bleuler, H., Cole, M., Keogh, P., Larsonneur, R., Maslen, E., Okada, Y. and Traxler, A., Magnetic bearings: theory, design, and application to rotating machinery (2009), Springer Science & Business Media.

Caple, M., Maslen, E., Nagel, J. and Wild, J., Control of an AMB to Zero Static Force, Proceedings of the 15th International Symposium on Magnetic Bearings (2016).

Cloud, C., Li, G., Maslen, E. H., Barrett, L. E. and Foiles, W. C., Practical applications of singular value decomposition in rotordynamics, Australian journal of mechanical engineering, Vol.2, No.1 (2005), pp.21-32.

Dawson, M., Childs, D., Holt, C., Phillips, S., Theory Versus Experiments for the Dynamic Impedances of Annular Gas Seals: Part 2 - Smooth and Honeycomb Seals, ASME J. Eng. Gas Turbines Power Vol.24 (2002), pp.963-970.

Hirschmanner, M., and Springer, H., Adaptive vibration and unbalance control of a rotor supported by active magnetic bearings, Proceedings of the 8th International Symposium on Magnetic Bearings (2002).

ISO 14839-3, Vibration of rotating machinery equipped with active magnetic bearings Part 3: Evaluation of stability margin, International Standards Organization (2006).

Jeong, S., Doyiung, J., Yongbok, L., Rotordynamic Behavior and Rigid Mode Vibration Control by Hybrid Foil-Magnetic Bearing System, Proceedings of the 15th International Symposium on Magnetic Bearings (2016).

Lang, O., Wassermann, J. and Springer, H., Adaptive vibration control of a rigid rotor supported by active magnetic bearings, Journal of engineering for gas turbines and power, Vol.118, No.4 (1996), pp.825-829.

Lauridsen, J. S., Sekunda, A. K., Santos, I. F. and Niemann, H., Identifying parameters in active magnetic bearing system using LFT formulation and Youla factorization, In: 2015 IEEE Conference on Control

[DOI: 10.1299/mej.16-00618]

Applications (2015), pp.430-435.
Maslen, E., Cloud, C., Hauge, T., Tarald, S. and Lie, J., Unbalance Response Assessment of a Subsea Compressor, Proceedings of the 13th International Symposium on Magnetic Bearings (2012).
Mushi, S. E., Lin, Z., Allaire, P. and Evans, S., Aerodynamic cross-coupling in a flexible rotor: Control design and implementation, Proceedings of the 11th International Symposium on Magnetic Bearings (2008).
Nelson, H. D., A finite rotating shaft element using Timoshenko beam theory, Journal of mechanical design, Vol.102, No.4 (1980), pp.793-803.
Nielsen, K. K., Joenck, K. and Underbakke, H., Hole-Pattern and Honeycomb Seal Rotordynamic Forces: Validation of CFD-Based Prediction Techniques, Journal of Engineering for Gas Turbines and Power Vol.134, No.12 (2012).
Pesch, A. H. and Sawicki, J. T., Stabilizing Hydrodynamic Bearing Oil Whip With mu-Synthesis Control of an Active Magnetic Bearing, In: ASME Turbo Expo 2015: Turbine Technical Conference and Exposition. American Society of Mechanical Engineers (2015), V07AT31A029-V07AT31A029.
Schonhoff, U., Luo, J., Li, G., Hilton, E. and Nordmann, R., Implementation results of mu-synthesis control for an energy storage flywheel test rig, Proceedings of the 8th International Symposium on Magnetic Bearings (2000).
Skogestad, S. and Postlethwaite, I., Multivariable feedback control: analysis and design, Vol. 2 (2007), New York: Wiley.
Wurmsdobler, P. and Springer, H., State space adaptive control for a rigid rotor suspended in active magnetic bearings, Proceedings to the 5th International Symposium on Magnetic Bearings (1996), pp.185-190.
Zhou, K., Doyle, J. C. and Glover, K., Robust and optimal control (1996), New Jersey: Prentice hall.

[DOI: 10.1299/mej.16-00618]